Research Article | Vol. 25, No. 4 | 20 Feb 2017 | OPTICS EXPRESS 3222

Optics EXPRESS

Characterization of digital dispersive spectrometers by low coherence interferometry

Ó. MARTÍNEZ-MATOS,[1,*] C. RICKENSTORFF,[1] S. ZAMORA,[1] J.G. IZQUIERDO,[2] AND P. VAVELIUK[3]

[1]*Departamento de Óptica, Facultad de Ciencias Físicas, Universidad Complutense de Madrid, 28040, Madrid, Spain*
[2]*Departamento de Química Física I and Centro de Laseres Ultrarrápidos, Facultad de Ciencias Quimicas, Universidad Complutense de Madrid, 28040, Madrid, Spain*
[3]*Centro de Investigaciones Opticas (CONICET La Plata-CIC), Cno. Centenario y 506, P.O. Box 3, 1897 Gonnet, Argentina*
[*]*omartine@fis.ucm.es*

Abstract: We propose a procedure to determine the spectral response of digital dispersive spectrometers without previous knowledge of any parameter of the system. The method consists of applying the Fourier transform spectroscopy technique to each pixel of the detection plane, a CCD camera, to obtain its individual spectral response. From this simple procedure, the system-point spread function and the effect of the finite pixel width are taken into account giving rise to a response matrix that fully characterizes the spectrometer. Using the response matrix information we find the resolving power of a given spectrometer, predict in advance its response to any virtual input spectrum and improve numerically the spectrometer's resolution. We consider that the presented approach could be useful in most spectroscopic branches such as in computational spectroscopy, optical coherence tomography, hyperspectral imaging, spectral interferometry and analytical chemistry, among others.

OCIS codes: (300.6190) Spectrometers; (120.6200) Spectrometers and spectroscopic instrumentation; (070.4790) Spectrum analysis; (110.4100) Modulation transfer function; (110.4850) Optical transfer function; (120.3180) Interferometry.

References and links

1. K. Liu and F. Yu, "Accurate wavelength calibration method using system parameters for grating spectrometers," Opt. Eng. **52**, 013603 (2013).
2. C. E. Cramer, S. Brown, N. Caldwell, A. K. Dupree, S. G. Korzennik, K. R. Lykke, and A. Szentgyorgyi, "A tunable laser system for the wavelength calibration of astronomical spectrographs," in Proceedings of IEEE Conference on Lasers and Electro-Optics and Conference on Quantum electronics and Laser Science Conference (IEEE, 2009) pp. 1–2.
3. R. de la Fuente, "White light spectral interferometry as a spectrometer calibration tool," Appl. Spectrosc. **68**, 525–530 (2014).
4. J.-H. Kim, J.-H. Han, and J. Jeong, "Accurate wavelength calibration method for spectrometer using low coherence interferometry," J. Lightwave Technol. **33**, 3413–3418 (2015).
5. R. C. Youngquist, S. M. Simmons, and A. M. Belanger, "Spectrometer wavelength calibration using spectrally resolved white-light interferometry," Opt. Lett. **35**, 2257–2259 (2010).
6. J. Serrano, J. Moros, and J. Laserna, "Exploring the formation routes of diatomic hydrogenated radicals using femtosecond laser-induced breakdown spectroscopy of deuterated molecular solids," J. Anal. At. Spectrom. **30**, 2343–2352 (2015).
7. C. Dorrer, "Influence of the calibration of the detector on spectral interferometry," J. Opt. Soc. Am. B **16**, 1160–1168 (1999).
8. M. Wojtkowski, "High-speed optical coherence tomography: basics and applications," Appl. Opt. **49**, D30–D61 (2010).
9. P. Wang and R. Menon, "Computational spectrometer based on a broadband diffractive optic," Opt. Express **22**, 14575–14587 (2014).
10. P. Wang and R. Menon, "Computational spectroscopy via singular-value decomposition and regularization," Opt. Express **22**, 21541–21550 (2014).
11. Z. Hu, Y. Pan, and A. M. Rollins, "Analytical model of spectrometer-based two-beam spectral interferometry," Appl. Opt. **46**, 8499–8505 (2007).

#279752 https://doi.org/10.1364/OE.25.003222
Journal © 2017 Received 10 Nov 2016; revised 11 Dec 2016; accepted 28 Dec 2016; published 7 Feb 2017

Optics EXPRESS

12. M. Iliev, A. K. Meier, B. Galloway, D. E. Adams, J. A. Squier, and C. G. Durfee, "Measurement of energy contrast of amplified ultrashort pulses using cross-polarized wave generation and spectral interferometry," Opt. Express **22**, 17968–17978 (2014).
13. A. Emadi, H. Wu, G. Graff, and R. Wolffenbuttel, "Design and implementation of a sub-nm resolution microespectrometer based on a linear-variable optical filter," Opt. Express **20**, 489–507 (2012).
14. P. Wang and R. Menon, "Ultra-high-sensitivity color imaging via a transparent diffractive-filter array and computational optics," Optica **2**, 933–939 (2015).
15. B. Redding and H. Cao, "Using a multimode fiber as a high-resolution, low-loss spectrometer," Opt. Lett. **37**, 3384–3386 (2012).
16. B. Redding, S. F. Liew, R. Sarma, and H. Cao, "Compact spectrometer based on a disordered photonic chip," Nat. Photon. **7**, 746–751 (2003).
17. V. J. Coates and H. Hausdorff, "Interferometric method of measuring the spectral slit width of spectrometers," J. Opt. Soc. Am. **45**, 425–430 (1955).
18. T. Katayama and A. Takahashi, "Optical transfer function of concave grating spectrometer based on wave optical method," Jpn. J. Appl. Phys. **9**, 1509 (1970).
19. H. Fujiwara, "Transfer function of spectroscopic systems using a sinusoidally modulated spectrum," J. Opt. Soc. Am. **71**, 238–242 (1981).
20. V. N. Kumar and D. N. Rao, "Two-beam interference experiments in the frequency-domain to measure the complex degree of spectral coherence," J. Mod. Opt. **48**, 1455–1465 (2001).
21. J. E. Stewart, "Polarization interferometer for the determination of spectral modulation transfer functions of monochromators," Appl. Opt. **6**, 1523–1525 (1967).
22. P. Hlubina, "Dispersive spectral-domain two-beam interference analysed by a fibre-optic spectrometer," J. Mod. Opt. **51**, 537–547 (2004).
23. R. Chelebus, P. Hlubina, and D. Ciprian, "Dispersion measurements of anisotropic materials and a new fiber-optic sensor configuration," Proc. SPIE **6609**, 66090H1 (2007).
24. P. Hlubina, V. Chugunov, and I. Gurov, "Dispersion compensation in temporal fourier holography and spectral fringe phase retrieval using a phase-locked loop method," Proc. SPIE **5481**, 120–128 (2003).
25. P. Hlubina and W. Urbanczyk, "Dispersion of the group birefringence of a calcite crystal measured by white-light spectral interferometry," Meas. Sci. Technol. **16**, 1267 (2005).
26. P. Hlubina, D. Ciprian, and L. Knyblová, "Interference of white light in tandem configuration of birefringent crystal and sensing birefringent fiber," Opt. Commun. **260**, 535–541 (2006).
27. P. Hlubina, D. Ciprian, and M. Kadulová, "Measurement of chromatic dispersion of polarization modes in optical fibres using white-light spectral interferometry," Meas. Sci. Technol. **21**, 045302 (2010).
28. P. Hlubina, D. Ciprian, J. Luňáňek, and M. Lesňák, "Dispersive white-light spectral interferometry with absolute phase retrieval to measure thin film," Opt. Express **14**, 7678–7685 (2006).
29. P. Hlubina, D. Ciprian, J. Luňáček, and R. Chlebus, "Phase retrieval from the spectral interference signal used to measure thickness of SiO2 thin film on silicon wafer," Appl. Phys. B **88**, 397–403 (2007).
30. B. M. Akca, V. D. Nguyen, J. Kalkman, N. Ismail, G. Sengo, F. Sun, A. Driessen, T. G. VanLeeuwen, M. Pollnau, K. Wörhoff, and R. M. Ridder, "Toward spectral-domain optical coherence tomography on a chip," IEEE J. Sel. Top. Quantum Electron. **18**, 1223–1233 (2012).
31. A. R. Korb, P. Dybwad, W. Wadsworth, and J. W. Salisbury, "Portable fourier transform infrared spectroradiometer for field measurements of radiance and emissivity," Appl. Opt. **35**, 1679–1692 (1996).
32. K. Kozima, H. Kanamori, and O. Matsuda, "Direct measurement of optical transfer functions of spectroscopic systems," JPN. J. Appl. Phys. **17**, 1271 (1978).
33. W. Frank, K. Goerke, and M. Pietralla, "Demonstrating fourier transform spectroscopy for students," Appl. Opt. **17**, 1413–1417 (1978).

1. Introduction

Spectroscopy is a extremely sensitive measurement technique that has been applied to virtually all fields of science and technology. In most cases, the usual choice for near UV, visible and near infrared analysis are dispersive spectrometers. Spectrometer characterization, i.e. wavelength calibration and resolution, ensures the correct operation of the device and provides its optical performance. Wavelength calibration is easily performed using input light with well known spectra, such as the light from a calibrated discharge lamp [1], tunable lasers [2], and the channeled spectrum from a Michelson Interferometer [3–5]. In contrast, characterization of the spectral resolution of spectroscopic systems is a more difficult and complex task. As a consequence, commercial digital dispersive spectrometers operating in a wide spectrum range have spectral resolutions roughly estimated. This is not an inconvenience for low resolution measurements but it is no longer acceptable for high resolution applications such as Laser Induced Breakdown

Optics EXPRESS

Spectroscopy [6], Spectral Interferometry [7] and Optical Coherence Tomography [8].

The spectral resolution of spectroscopic systems can be determined by means of the Point Spread Function (PSF). The spatial-PSF [9, 10] is the intensity spatial profile in the detector plane corresponding to a single wavelength [11]. The dispersive element of a spectrometer (a prism or grating), maps input signals of different wavelengths to specific spatial locations in the detector plane. Therefore, each detection point receives a finite spectral contribution dependent on the spectrometer's dispersion and the extension of the spatial-PSF. The spectral intensity arriving at each point is called the spectral-PSF [9, 10]. The challenge in the characterization of digital dispersive spectrometers is to obtain the spectral-PSF with very high accuracy and to take into account the effect of the pixel width. The combination of both effects gives rise to the spectral response of the spectrometer.

Different methods have been proposed to determine the PSF in spectroscopic systems. Direct methods involve the measurement of the spatial-PSF by grating scanning [12] or by using the output light of a monochromator [13], while the spectral-PSF has been measured by spectrum analysis at every pixel in the detector array using a secondary spectrometer [9, 10, 14] or a tunable laser [15, 16]. While the first three methods are not very accurate, the last one involves the use of tunable lasers which are expensive, require calibration and are limited by the tuning range. The most important indirect approach is based on low coherence (white light) interferometry [17–21] for the determination of monochromator's spectral-PSF. In this method, the monochromator is illuminated with a sinusoidally modulated spectrum from the output of a Michelson or a Fabry-Perot interferometer. The contrast of the spectrogram gives rise to the Modulation Transfer Function (MTF) from which the spectral-PSF is obtained via the Fourier Transform (FT). This last relation is valid only when the Optical Transfer Function (OTF) is real and positive, but in most of the cases this assumption is taken for granted without proper verification. The indirect approach has also been extended to digital dispersive spectrometers. In [22], a Gaussian spectral-PSF model was introduced and has been employed to find dispersion properties of materials [23–27] and material thickness [28,29] involving the use of Spectral Interferometry. By other side, a Gaussian model for the spatial-PSF that takes into account the pixel width was proposed in [11]. This last model has been used to explain the visibility roll-off in Optical Coherence Tomography [30]. Even if these approximations worked well in some cases they can not be generalized to all spectrometers since its spatial and spectral-PSFs could depart from a Gaussian function. This clearly shows that the spectral response should be found experimentally in each individual element of the detection array to get a full insight of a particular digital dispersive spectrometer.

In this work, we apply the Fourier Transform Spectroscopy (FTS) technique to determine the spectral response at each pixel of a digital dispersive spectrometer. The proposed method is low cost, provides arbitrarily high spectral resolution, characterizes the spectrometer in its working configuration, does not require previous knowledge of the device's optical elements and it provides a full description that incorporates the effects of misalignment, aberrations and finite pixel width. These advantages make our proposal very attractive for a broad range of spectroscopic applications.

2. Experimental method and setup

A digital dispersive spectrometer is schematically represented in Fig. 1. This is a 4f system with an entrance slit on the Object Plane, a CCD or CMOS camera on the Image Plane and a grating on the Fourier Plane. The FTS technique applied to each pixel of the detector array is performed by means of a Michelson interferometer with a movable mirror located in front of the spectrometer, as Fig. 1 shows. A time delay, τ, introduced by moving one of the mirrors with a linear stage motor, provides a sinusoidally modulated spectrum at the input of the spectrometer. One recorded image for a fixed τ, and the corresponding normalized intensity profile are shown

Optics EXPRESS

in the Inset 1 of Fig. 1. Notice that in the arrangement a broad bandwidth source 350-700 nm is used as the spectrometer's source. The temporal signal registered by one individual pixel as a function of τ is shown in the Inset 2 of Fig. 1. The Fourier Transformation of this temporal signal yields the spectral response at each detection element, whose shape and form is dictated by both the spectral-PSF and the pixel width. The collection of all the pixel responses gives us the Response Matrix, whose rows are pixels, columns are frequencies (wavelengths) and the values spectral intensities. The Response Matrix fully characterizes the spectrometer.

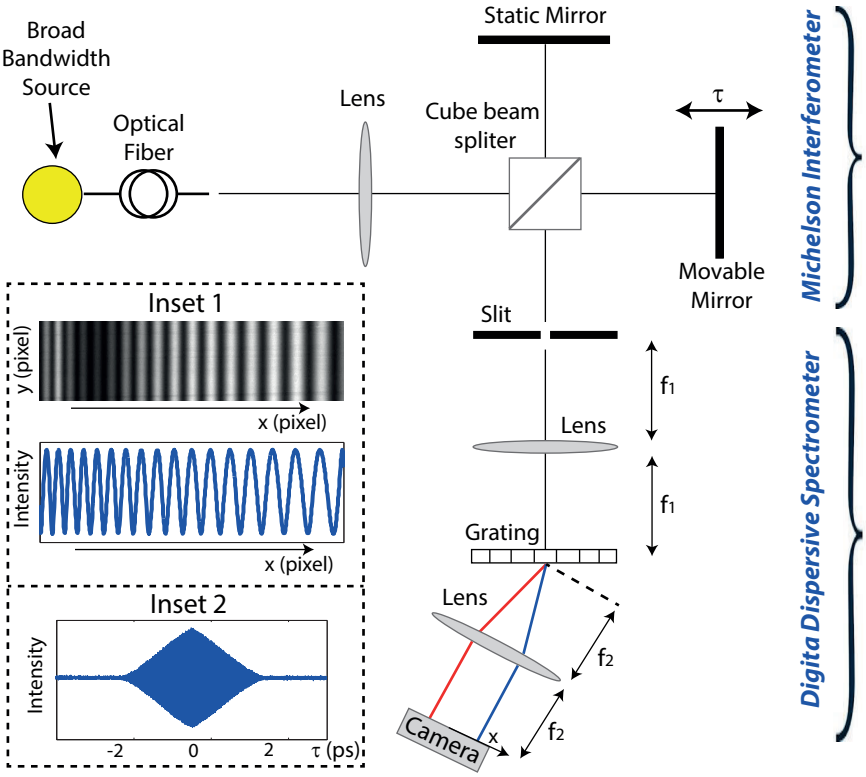

Fig. 1. Experimental setup to characterize a digital dispersive spectrometer. The Michelson Interferometer is used to illuminate the spectrometer with a time dependent interference pattern. Inset 1: photograph recorded by the camera and its normalized intensity profile. Inset 2: temporal signal recorded by an individual pixel as a function of the time delay. The Fourier transformation of this signal is the spectral response at each pixel, that represents a column vector in Fig. 2(b).

It is well known that FTS technique applied to the visible and UV spectral regions is very sensitive to small perturbations such as vibrations and temperature gradients. These perturbations slightly modify the carrier of the temporal signal registered by each pixel, producing catastrophic and unreal effects on the spectrum after Fourier transformation. Applying the FTS technique directly requires highly isolated conditions that reduces the applicability of the proposed approach. In order to overcome this limitation, and be able to work in a non-isolated environment, the FTS technique should be adapted to our experiment. In virtue that each pixel receives a symmetric and narrow spectral bandwidth (demonstrated below), the pixel's temporal signal consists on a symmetric envelope, the |OTF|, with a constant carrier frequency. The absence of frequency chirp in the oscillatory part of the signal implies that the OTF is real. Then, this function is obtained from the |OTF| assigning a sign change every time the |OTF| intercepts the zero

Optics EXPRESS

value. Taking into account that the OTF is insensitive to small perturbations while the carrier frequency is extremely sensitive, it is convenient to analyze each part of the signal separately. Once this has been done, the complete temporal signal at each pixel is obtained assigning the corresponding carrier frequency to its OTF. The Fourier Transform of this signal gives the same results than directly applying the FTS technique with the advantage of reducing the isolation constrains significantly and hence the cost of the device.

In order to determine the Response Matrix, first we must find the carrier frequency, $\nu(x)$, associated to each pixel position, x, which is known as the calibration curve. To this aim, we analyze the interference in the spectral domain of two beams emerging from the Michelson Interferometer for a time delay τ, following the method proposed in [3,4]. The intensity profile at the camera, $S(x,\tau)$, is:

$$S(x,\tau) = I[\nu(x)]\{1 + f[\nu(x),\tau]\cos(4\pi\nu(x)\tau)\} \tag{1}$$

where $I[\nu(x)]$ is the broad bandwidth input source and $f[\nu(x),\tau]$ is the fringe visibility due to the PSF and the effect of the finite pixel width. Function $f[\nu(x),\tau]$ evaluated at pixel x is the OTF for that pixel as a function of time τ. The argument $\phi(x)$ in the oscillatory part in Eq. (1) is found from the normalized intensity profile shown in the Inset 1 of Fig. 1 just taking the acos(.) and then unwrapping. By this procedure the carrier frequency $\nu(x) = \phi(x)/(4\pi\tau)$ at each pixel of the camera is obtained without interpolation or fitting techniques. We choose τ for calibration instead of fitting $\phi(x)$ to discrete spectral values, as proposed by [3], because it can be accurately measured in our experiment. Our approach needs only a known spectral line, i. e. a He-Ne laser, to provide the offset adjustment by associating a known frequency to a fixed pixel position.The two approaches give very similar results. The accuracy of the procedure to find the calibration curve will be checked in the next section.

3. Response matrix of digital dispersive spectrometers

We measure the Response Matrix of three digital dispersive spectrometers possessing different spectral response regimes. To describe these regimes, we employ diffraction theory to find the PSF for a perfectly aligned aberration free system:

$$PSF(x,\lambda) \sim \left|\mathrm{rect}\left(-\frac{f_1}{f_2}\frac{x}{a}\right) \otimes \mathrm{sinc}\left[b\left(\frac{x}{\lambda f_2} - \frac{1}{\Lambda}\right)\right]\right|^2, \tag{2}$$

where rect(.) and sinc(.) are the usual rectangular and sinc functions that represent the slit image and the FT of the grating pupil. Parameters a, b, f_1, f_2 and Λ are the slit width, the grating width, focal length of lens 1 and 2, and the grating period, respectively, and $\otimes$ is the convolution operation. The spectral intensity of the light source has been considered constant in Eq. (2) since it varies slowly in the spectral response range of each pixel. The spectral response regimes can be derived attending to which convolving function dominates in Eq. (2). In this way, the PSFs approximately behave as

$$\left|\mathrm{rect}\left(-\frac{f_1}{f_2 a}\left(x - \frac{\lambda f_2}{\Lambda}\right)\right)\right|^2, \tag{3}$$

when the slit image dominates, as

$$\left|\mathrm{sinc}\left[b\left(\frac{x}{\lambda f_2} - \frac{1}{\Lambda}\right)\right]\right|^2, \tag{4}$$

when the FT of the grating pupil dominates and as the general case Eq. (2) for similar contributions. In this work we adjust a and b experimentally to obtain the OTFs for each of the

Optics EXPRESS

three behaviors mentioned above. Since the OTF is linked to the spectral-PSF via the Fourier Transform, spectrometers S1-S3 are designed to follow a temporal signal that match the FT's shape of Eqs. (3), (4) and (2), i. e. sinc(.), tri(.) and FT [Eq. (2)], respectively. The tri(.) is the usual triangular function. The slit and grating width that experimentally satisfy these temporal behaviors are shown in Table 1. The common parameter values for the three spectrometers are: grating of 300 lines/mm; f_1 = 15 cm and f_2 = 7.5 cm. The three spectrometers are made from the same optical setup in Fig. 1 varying the slit and grating width values. The slit width is changed with an adjustable slit, while the grating width is changed using an adjustable iris located at the Fourier Plane, placed in physical contact with the grating.

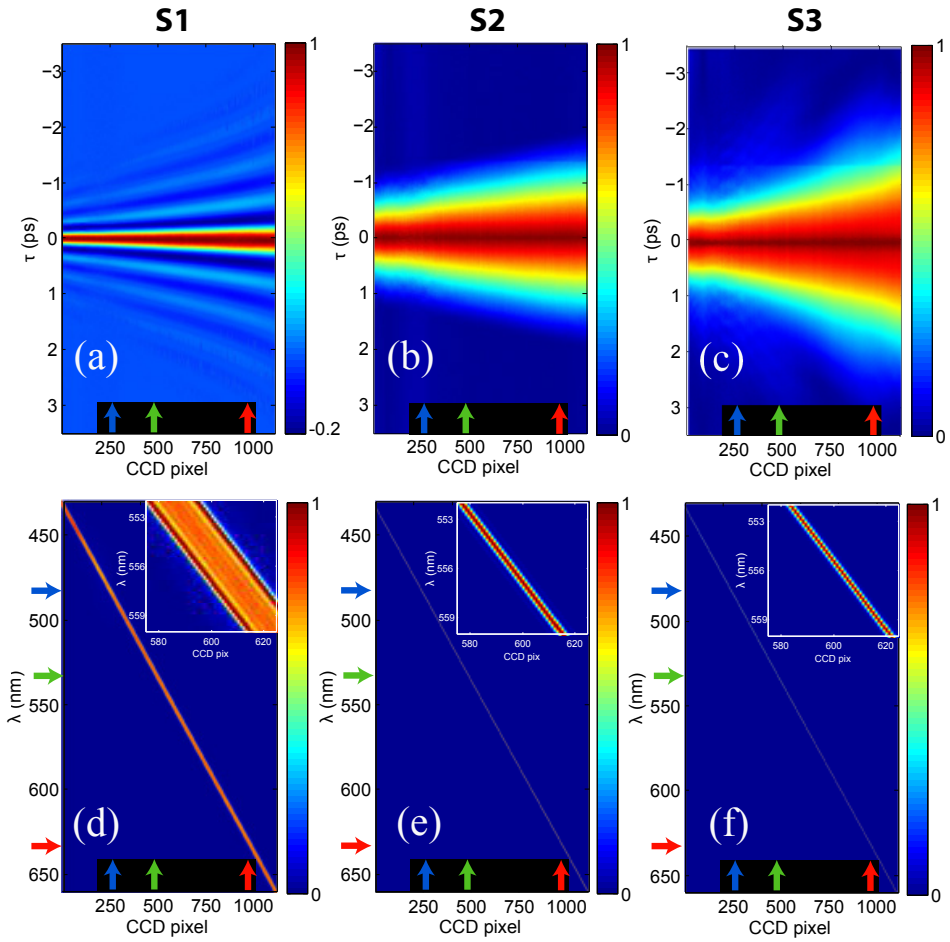

Fig. 2. OTF registered by each pixel of the camera, (a)-(c), for spectrometers S1-S3, respectively. Response Matrix and a zoom around pixel number 600, (d)-(f), for spectrometers S1-S3, respectively. The Response Matrix is calculated by Fourier transforming the OTF at each pixel and centering the spectrum to its carrier frequency. The vertical and horizontal arrows indicate the cross-section directions in Fig. 3 (OTFs and the spectral response) and in Fig. 5 (spatial response), respectively.

The experimental results for the three spectrometers are shown in Fig. 2. Figures 2(a)-2(c) represent the OTF registered by each pixel of the camera as a function of τ for S1-S3, respectively. Figures 2(d)-2(f) show the Fourier Transformation of the OTF evaluated at each pixel and centered at its carrier frequency, i.e. the Response Matrix. In Figs. 2(e)-2(f) the matrix re-

Optics EXPRESS

Table 1. Slit and grating width for the three spectrometers, S1-S3.

Spectrometer	*a* (mm)	*b* (mm)
S1	0.24	25
S2	0.02	2
S3	0.02	25

sponse comprises a thin central lobe clearly visible in the online version. The inset in the upper corner on these figures helps to visualize the spectral response of the spectrometers for a few CCD pixels. By this simple procedure the spectral response at each detection element is found with a precision of ~ 0.04 nm. This value is the spectral increase between consecutive points in Figs. 3(b), 3(d) and 3(f). Since this value is inversely proportional to the temporal signal length (not shown at full length in the figure), the precision to determine the spectral response of the spectrometer can be increased by just measuring a longer time delay. It is important to note that the spectrometer, as a whole, acts a "Black Box" for the proposed procedure. In this sense, the Response Matrices are completely general, found without a previous knowledge of any parameter of the system.

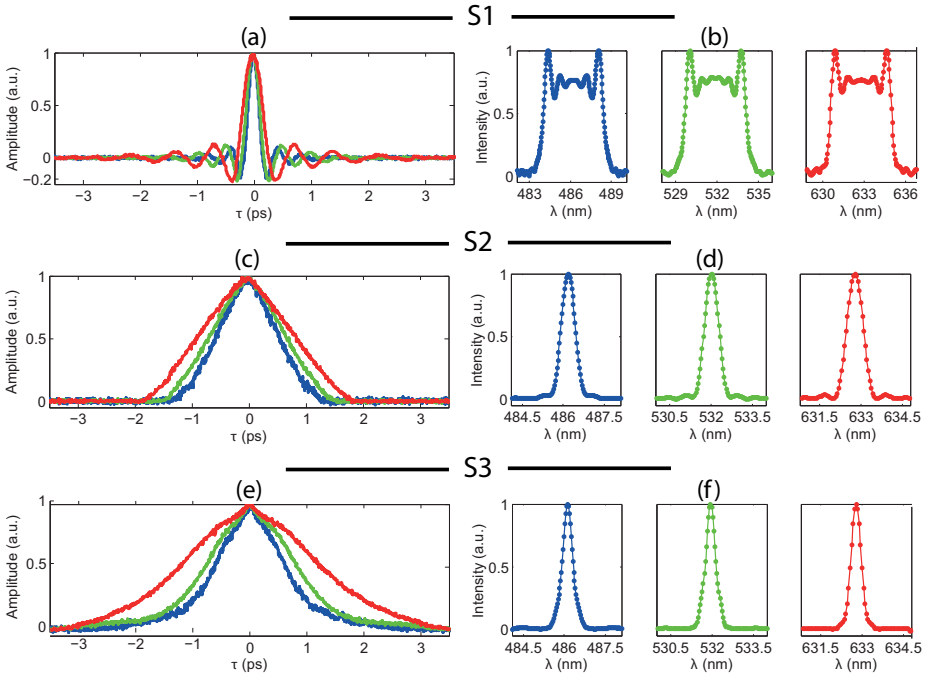

Fig. 3. Figures (a), (c) and (e) are the OTFs corresponding to the vertical cross-sections of Figs. 2(a)-2(c), respectively. Figures (b), (d) and (f) are the spectral response corresponding to the vertical cross-sections of Figs. 2(d)-2(f), respectively. The cross-sections are evaluated at the positions pointed by the vertical arrows in Fig. 2. The color lines in the figure are correlated with the color arrows in Fig. 2. The spectrum is analyzed around wavelengths λ =486.1 nm, 532.0 nm and 632.8 nm.

The vertical cross-sections pointed by the vertical arrows in Fig. 2 are shown in Fig. 3 for the three spectrometers. Figures 3(a), 3(c) and 3(e) are the OTFs for S1-S3, while Figs. 3(b), 3(d) and 3(f) are the spectral responses for S1-S3, respectively. The cross-sections are centered around wavelengths λ =486.1 nm, 532.0 nm and 632.8 nm. It can be seen that the experimen-

Optics EXPRESS

tal OTFs for S1 and S2 clearly resemble the sinc(.) and tri(.) functions and its corresponding spectral responses follow the $|\text{rect}(.)|^2$ and $|\text{sinc}(.)|^2$ functions, in accordance with the spectrometer's design. The experimental results in Figs. 3(b) and 3(d) indicate that the method recovers the fine details of the spectral response, i.e., the local maximum and minimum on top of the rectangular shape for S1, and the secondary maximum and minimum of the $|\text{sinc}(.)|^2$ function for S2.

In order to validate the theoretical PSF model, we compare the spatial extension of the convolving functions in Eq. (2) using the values given in Table 1. To this aim, we define the spatial width relation $\alpha = W_{rect}/W_{sinc} = a\,b/\,(0.88\,\lambda\,f_1)$, where W_{rect} and W_{sinc} are the FWHM of Eqs. (3) and (4), respectively. The α-values evaluated at $\lambda = 500$ nm are $\alpha_1 = 90$, $\alpha_2 = 0.6$ and $\alpha_3 = 7.5$ for S1-S3, showing that the dominant term in Eq. (2) is clearly the slit image for S1 and S3, while for S2 the slit image and the FT of the grating pupil have similar contributions. These results contradict the experimental behavior found in Figs. 2-3, in which the slit image dominates in S1, the FT of the grating pupil dominates in S2 and both have the same contribution in S3. We conclude that the simplified model Eq. (2) is incomplete since it does not consider the effect of the pixel width and the assumption of a perfectly aligned free aberration spectrometer is not satisfied. Moreover, in none of the cases analyzed in this work does the spectral-PSF, nor the spatial-PSF, have a Gaussian response as it is usually assumed. Taking this into account and realizing that the system imperfections are very tricky to account theoretically, it is mandatory to find experimentally the Spectral Response of digital dispersive spectrometers for a proper description of the device.

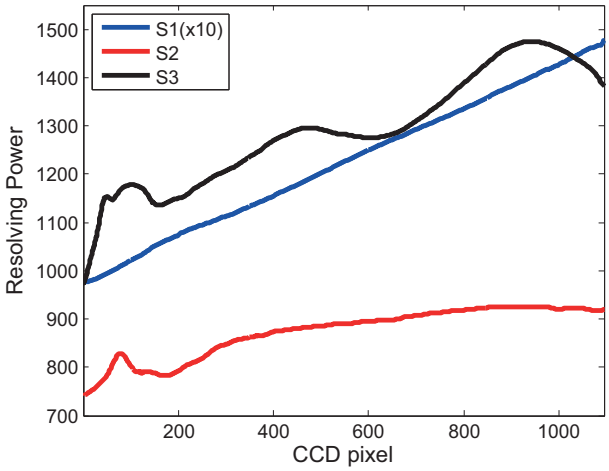

Fig. 4. Resolving power for the three spectrometers evaluated at each pixel of the camera. The curve for S1 has been magnified for easy viewing.

According to the generalization of the Rayleigh criterion, the resolving power, R, of a digital dispersive spectrometer evaluated at each pixel x_i is $R(x_i) = \lambda_c(x_i)/\lambda_{FWHM}(x_i)$, where $\lambda_c(x_i)$ is the central wavelength at x_i determined by the calibration curve and $\lambda_{FWHM}(x_i)$ is the FWHM of the spectral response at x_i. The resolving power as a function of the pixel number for the three spectrometers is shown in Fig. 4. It can be seen that S1, with an approximated constant value $\lambda_{FWHM}(x_i)$ has a resolving power proportional to the wavelength (and to the pixel number), while S2, whose $\lambda_{FWHM}(x_i)$ value is proportional to $\lambda_c(x_i)$ has an approximately constant R dependence. The behavior for S3 is not easily deduced due to a more complex spectral response. Nevertheless, the detailed information given by R is crucial for high resolution

Optics EXPRESS

spectroscopy in which the spectrometer can have local variations in the resolving power. Even in the case of S2, whose behavior approximates to an ideal spectrometer, the spectral response is not constant for all pixels as it is presupposed for most commercial spectrometers. Moreover, according to the classical text books, the R value is found as the product of the grating frequency in lines/mm, times the grating extension in mm, giving a wrong result $R = 600$ for S2. These results support the necessity of finding R experimentally.

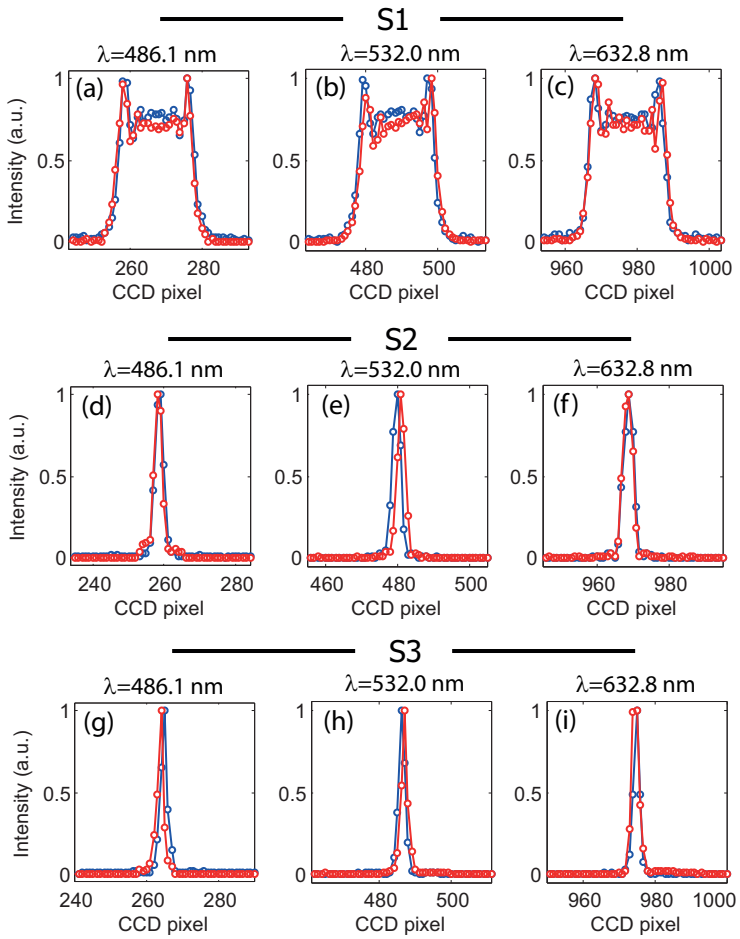

Fig. 5. Comparison of the horizontal cross-sections of Fig. 2, blue lines, with the image recorded directly by the camera, red lines, under quasy-monochromatic illumination. The cross-sections are indicated by the horizontal arrows in Fig. 2, corresponding to λ =486.1 nm, 532.0 nm and 632.0 nm. The quasy-monochromatic sources are the spectral line of a hydrogen discharge lamp centered at 486.1 nm, a solid state laser emitting at 532.0 nm and He-Ne laser emitting at 632.8 nm. Figures (a)-(c) are the results for S1, Figs. (d)-(f) for S2 and Figs. (g)-(i) for S3.

In Fig. 5 we check the validity of the approach comparing the spatial responses found by the Response Matrix and by an alternative method. Blue lines in Fig. 5 are the horizontal cross-sections of the Response Matrix (the spatial response) evaluated at λ =486.1 nm, 532.0 nm and 632.8 nm. These positions are indicated by the horizontal arrows in Fig. 2. Figures 5(a)-5(c) show the cross-sections for S1, while Figs. 5(d)-5(f) and Figs. 5(g)-5(i) show the cross-sections for S2 and S3, respectively. We compare these results with the intensity profiles registered

Optics EXPRESS

by each spectrometer under quasy-monochromatic illumination. Each quasy-monochromatic signal is also the spatial response for that wavelength. Red lines in Fig. 5 correspond to the spectral line of a hydrogen discharge lamp (486.1 nm), a solid state laser (532.0 nm) and a He-Ne laser (632.8 nm). These three light sources can be considered monochromatic since the FWHM of their spectral lines is much smaller than the resolution of any of the spectrometers analyzed. The shape, width and position measured by the two methods are in good agreement, demonstrating that our procedure works properly. The results in Fig. 5 also show that the three spectrometers have a symmetric spatial response. Taking into account that a narrow symmetric spectral response leads to a symmetric spatial response for linear dispersion spectrometers we conclude that the assumption of spectrum symmetry is fully satisfied. Even in the case in which this condition is not met the proposed method still applies, but in this hypothetical case the OTF is complex giving rise to a temporal signal with non-constant carrier frequency. The oscillatory part of the signal should be carefully measured to obtain the imaginary part of the OTF. To this aim, a proper setup isolation or a reference laser line would be necessary to take into account the slight variations in the mirror displacement. This last solution is commonly used in infrared Fourier Transform Spectroscopy [31]. Fortunately, the condition of symmetry is satisfied in most spectrometers.

In addition, the experimental results in Fig. 5 confirm the validity of the method employed to find the calibration curves. The maximum discrepancy in the spatial position is one pixel, which is the best precision that can be reached for the wavelength calibration method. This limitation comes from the accurateness in finding the He-Ne peak's intensity used for the calibration process, which is one pixel. According to the spectrometer dispersion, one pixel error corresponds to a maximum wavelength error of ~0.2 nm for the whole spectral range. This is a very good result compared to standard methods.

4. Resolution enhancement

The Response Matrix can be employed to calculate the signal on the CCD camera for a particular input spectrum. To do so, we perform the matrix operation $\mathbf{S} = \mathbf{I} \cdot \mathbf{RM}$, where the output signal $\mathbf{S}$ is a N-dimension row vector, the input spectral intensity $\mathbf{I}$ is a M-dimension row vector and $\mathbf{RM}$ is the NxM dimension Response Matrix of the spectrometer. In the notation, N is the number of camera pixels and M is the number of discretization points of the spectral response. For simplicity the quantum efficiency of the sensor array is considered constant for all pixels. The mathematical calculation of $\mathbf{S}$ is straightforward, allowing us to estimate the spectrometer performance for any input spectrum before to carry out any experiment. We will show this when discussing Fig. 6. The Response Matrix can also be employed to increase numerically the resolution of the spectrometer, as demonstrated in [32] and in Computational Spectroscopy [9,10,15]. Accordingly, we should obtain $\mathbf{RM}^{-1}$ for $M = N$ or the generalize inverse matrix of $\mathbf{RM}$ for $M \neq N$. Here, we propose an alternative method appropiate for spectrum analysis of light sources with a few spectral lines that allows us to determine the lines width and central positions. This procedure is specially suitable for laser emmision and spectral displacement measurement of known spectral lines due to doppler effect. Let us define the Root Mean Square Difference, Δ:

$$\Delta(a_1, a_2, ..., a_n) = \frac{1}{N}\sqrt{\sum_{i=1}^{N}\left(S(x_i) - \sum_{j=1}^{M} I(\lambda_j, a_1, a_2, ..., a_n) RM(\lambda_j, x_i)\right)^2} \tag{5}$$

that quantifies the difference between the experimental signal measured by the spectrometer, $S(x_i)$, and the signal composed using $\mathbf{RM}$ and the input spectrum $I(\lambda_j, a_1, a_2, ..., a_n)$. The a_i values, that minimize Δ determine the best input spectrum that approximates more closely to the real input spectrum. Variable x_i is the spatial position of pixel number i. It is convenient

Optics EXPRESS

to use input spectrum functions with physical meaning, such as Lorentzian or Gaussian if, for example, the light emitted comes from a discharged lamp or a laser. In this case the parameters a_i determine the relative intensity, width and central wavelength of each spectral line. We employ the medium resolving power spectrometer, S2, to demonstrate a substantial improvement in its spectral resolution. Two examples are investigated: the spectrum of a solid state laser with FWHM close to the spectral resolution of S2, and the Sodium D-lines with a doublet spectral separation also close to the spectral resolution of S2. The input spectrum functions, the parameter values that minimize Δ, and the value Δ are summarized on Table 2.

Table 2. Test spectrum parameters.

Laser	Sodium D-lines
$I = A_0 \exp\left[-(\lambda - \lambda_0)^2/\delta\lambda^2\right]$	$I = \sum_{i=1}^{2} A_i \exp\left[-(\lambda - \lambda_i)^2/\delta\lambda^2\right]$
$A_0 = 1$	$A_1 = 1;\ A_2 = 0.72$
$\lambda_0 = 642.10$ nm	$\lambda_1 = 589.03$ nm; $\lambda_2 = 589.63$ nm
$\delta\lambda = 0.35$ nm	$\delta\lambda = 0.033$ nm
$\Delta = 0.006$	$\Delta = 0.004$

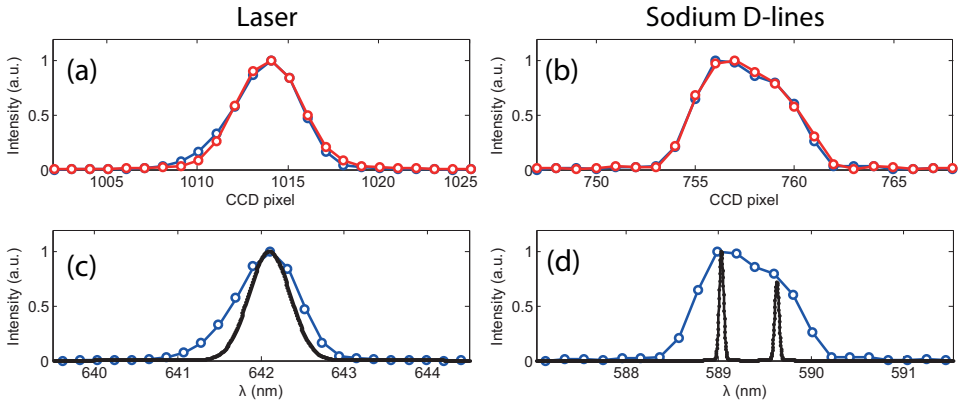

Fig. 6. Resolution enhancement results for spectrometer S2. Image recorded by the camera, blue lines, and the composed signal using the RM and the best input spectrum, red lines, for the laser (a) and the Sodium D-lines (b). Best input spectrum, black lines, and the experimental results expressed in wavelengths by means of the calibration curve, blue lines, for the laser (c) and the sodium D-lines (d).

Blue lines in Fig. 6(a)-6(b) are the signals recorded directly by the camera, while red lines are the composed signals using the $\mathbf{I} \cdot \mathbf{RM}$ operation. There is an optimal fitting between the two sets of lines. Blue and black lines in Fig. 6(c)-6(d) are the experimental results and the best input spectrum, $\mathbf{I}$, respectively. For proper comparison the blue lines in Fig. 6(c)-6(d) have been expressed in wavelengths instead of pixels by means of the calibration curve. The results for the laser show that the FWHM $= 2\sqrt{\ln 2}\delta\lambda = 0.58$ nm for the best input spectrum is smaller than the one measured directly, FWHM $= 0.9$ nm. This fact should be taken into account in order to determine spectral line widths. Otherwise, the coherence length of lasers or other light sources may be sub-estimated. When analyzing the sodium doublet, the S2 spectrometer's

Optics EXPRESS

Resolving Power evaluated at $\lambda = 589$ nm is $R = 890$, giving a spectral resolution of 0.7 nm, similar to the tabulated spectral separation of the sodium doublet. Therefore, the spectrometer itself is in the limit to distinguish the doublet without any numerical treatment. The spectral separation lies within 0.4 nm and 0.8 nm by simple inspection of Fig. 6(d) and 0.60 ± 0.04 nm using our procedure. The precision value 0.04 nm is the increment between two consecutive spectral points in **RM**, which can be enhanced just by measuring longer temporal signals or using interpolation. We estimate the FWHM $\sim$ 0.055 nm for each spectral line. It is in fact the upper limit for the FWHM, since smaller values give identical results for Δ. The values obtained for the Sodium are in accordance with the results in [33]. We would like to highlight that the exact position of each line differs slightly from the real one due to the one pixel error in the calibration curve, which is of the order of 0.2 nm, as discussed earlier. In summary, a low resolution spectrometer (R=890) can be improved by a factor 16x (R = 589nm/0.04nm = 15000) using our procedure. The spectral separation of close spectral lines as doublets and triplets, the FWHM of spectral lines, small spectral displacements due to Doppler Effect, and in general, fine spectral details, can be elucidated easily by employing the Response Matrix of the spectrometer.

5. Conclusions

We have proposed and demonstrated a useful procedure to determine the spectral response of digital dispersive spectrometers, the Response Matrix, that does not require a previous knowledge of the system parameters. The method takes into account the behavior of all the optical elements that compose the spectrometer including the effects of small misalignment, lens apertures, aberrations, optical imperfections and pixel width -all of them phenomena very tricky to determine properly. It can be said that the spectrometer, as a whole, acts as a "Black Box" for the proposed procedure. We showed that the spectrometer's spectral response in the range 350-700 nm can be determined with a precision of $\sim$ 0.04 nm. This value can be easily improved by just measuring longer temporal signals, opening the door to the characterization of very high resolving power dispersive spectrometers. It is also demonstrated that the Response Matrix can be employed to boost low resolving spectrometers to meet higher performance capabilities. For instance, we have shown how a spectrometer with $R \sim 890$ can resolve fine spectral details corresponding to $R \sim 15000$, such as the sodium doublet separation and the upper limit of the spectral FWHM of each spectral line, which is 0.055 nm. The procedure described in this work makes our proposal attractive for a broad range of spectroscopic applications.

Funding

Spanish Ministerio de EconomÃa y Competitividad (MINECO), project TEC2014-57394-P. CONACyT posdoctoral grant 266764.

Acknowledgments

We thank J. A. Rodrigo for valuable discussions and advice. PV acknowledges CNPq (Brasil).